Int. J. Electron. Commun. (AEÜ) 142 (2021) 153991

Contents lists available at ScienceDirect

International Journal of Electronics and Communications

journal homepage: www.elsevier.com/locate/aeue

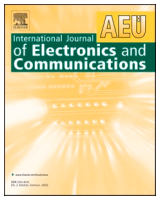

Regular paper

Correction of errors and harmonic distortion in pulse-width modulation of digital signals

Francisco Colodro *, Juana María Martínez-Heredia, José Luis Mora, Antonio Torralba

Electronic Engineering Department, ETS de Ingeniería, Universidad de Sevilla, Camino de los Descubrimientos s/n, 41092 Sevilla, Spain

ARTICLE INFO

Keywords:
Pulse-width modulation
Sigma-delta modulation
Digital-analog conversion

ABSTRACT

Pulse-Width (PW) modulation is widely used in those applications where an analog or digital signal has to be encoded in the time domain as a binary stream, such as switched-mode power amplifiers in transmitters of modern telecommunication standards, high-resolution digital signal conversion using single-bit digital-to-analog converters, and many others. Due to the fact that digital signals are sampled in the time domain, the quality of the resulting PW modulated waveforms is worsened by harmonic distortion. Multilevel PW modulation has been proposed to reduce these adverse effects, but the modulated waveform is no longer binary. In this paper, the mechanisms by which harmonic distortion is produced are analyzed. As a result, the distortion terms are mathematically quantified and used to correct the errors. Note that a correction network based on a simple subtraction of the distortion terms from the PW modulated signal would produce a waveform that would no longer be binary. The proposed correction network is implemented in the digital domain and, by means of a sigma-delta modulator, preserves the binary feature of the PW modulated output.

1. Introduction

Pulsewidth (PW) modulation is a sort of time encoding where analog or discrete multilevel values can be encoded into a two-level waveform. The duty cycle of this waveform is proportional to the encoded value. A PW modulated signal can be created by comparing the input signal to a reference wave of period $T_{PWM} = 1/F_C$ in such a way that the output takes a high value when signal is greater than the reference and a low value otherwise. Sawtooth or triangular waves are commonly used as that reference. PW modulation is called Naturally-sampled PW modulation (NPWM) when the input signal is continuous in the time domain. On the other hand, when a discrete-time (DT) signal is encoded, it is called Uniformly-sampled PW modulation (UPWM).

PW modulation has been widely used for electronic power conversion [1–4] and for the design of class-D amplifiers [5–7]. The spectrum of an NPWM signal can be decomposed into a DC offset, the low frequency components, which reproduce the input sigmal, and high frequency replicas around multiples of the carrier frequency F_C [7,8]. Thus, the input signal can be rebuilt by low-pass filtering. However, in addition to the aforementioned spectral components, the UPWM signal also contains harmonics of the input signal at low frequencies [7,9,10] so, despite the low-pass filtering, the input signal cannot be rebuilt without errors.

With the advent of the digital technologies, information processing has moved from the analog to digital world, and UPWM has been used more and more every day. One of the first application was in the field of audio. Beside the advantage of class-D amplifiers, which can be driven by a UPWM signal, in terms of power efficiency [5,6,9,11], it is also possible to implement a complete digital audio amplifier [7]. In principle, it could seem that this modulation does not allow to obtain high precision since a direct conversion of a 16-bits PCM audio signal to a UPWM signal would be require such a high sampling frequency f_s and reference frequency F_C that they would be no practical. Fortunately, it is possible to reduce the resolution of the digital signal to a much smaller number than 16 bits by using a sigma-delta modulator (SDM). More recently, interest in SDM-UPWM based digital-to-analog conversion (DAC) has increased in other fields of signal processing. UPWM has even been used as an inner module in the design of continuous-time (CT) SDMs to replace the inner quantizer or multibit DAC [12–16]. In the last years, PW modulation has also been used in optical and radio communication systems. In the first case to drive a laser in a radio-over-fiber architecture [17] or LEDs in indoor visible light communications [18]. In the second case [19–21], to drive the switched-mode power amplifier (SMPA) at the front-end of a transmitter. The SMPA is a very high

* Corresponding author.
E-mail addresses: pcolr@us.es (F. Colodro), jmmh@us.es (J.M. Martínez-Heredia), jolumo@us.es (J.L. Mora), torralba@us.es (A. Torralba).

https://doi.org/10.1016/j.aeue.2021.153991
Received 29 July 2021; Accepted 30 September 2021
Available online 9 October 2021

efficient circuit in terms of power consumption and the use of UPWM facilitates the digital design of the complete transmitter.

To obtain the performance required by the standards corresponding to the aforementioned applications, the harmonic distortion of the input signal produced by the UPWM has to be removed or reduced. Various techniques have been proposed in the literature. Harmonic distortion can reach an acceptable level by using multilevel PWM [10,16,19] but the output waveform is no longer binary, making it difficult to drive class D or SMPA amplifiers. Other techniques are based on the digital correction of the error [2,9] or on the prediction of the instant in which the unsampled input signal is equal to the reference wave [7,11,21]. These techniques are based on classical interpolators such as Lagrange, splines, and polynomials. More recently, Volterra series [22,23] and MAP and MMSE estimators [24] have been used to digitally reduce the error produced by the UPWM. An attempt has been also made to mathematically identify those spectral components which cause the error [25]; in this case, in addition to the computational complexity, the output signal is, once again, not binary.

In this paper, the mechanisms by which harmonic distortion is produced are analyzed. As a result, the distortion terms are mathematically identified and used to correct for errors. The correction procedure involves more than a simple subtraction of the distortion term to the PW modulated signal, which would lead to a non-binary modulated signal, as discussed earlier. The proposed correction network is implemented in the digital domain by means of a sigma-delta modulator that preserves the binary nature of the modulated output. The rest of paper is structured as follows. In section 2, UPWM is revised together with the mathematical equations [10] on which the proposed architecture is based. The proposed architecture is presented in section 3. Simulation results as well as a comparison with other correction methods are presented in section 4, and conclusions are drawn in section 5.

2. PW modulation of sampled signals

The PWM-based DAC is shown in Fig. 1.a and Fig. 1.b. In the former, the PWM is performed in the CT domain; in the latter, it is performed in the DT domain. Both systems are equivalent in the sense that they ideally produce the same output $v(t)$ [10]. The input $x(n)$ is a B-bandwidth, high resolution, k-bit PAM signal (where k is a large positive integer) sampled at the rate $f_s = 1/T$. The resolution is reduced by means of a m-bit SDM ($m < k$). Let L be the number of levels of $y(n)$, where L is not necessarily a power of two ($L \leqslant 2^m$). To encode without errors each of these L levels in Fig. 1b, it is necessary to divide the period T in $F = L - 1$ time slots. Then, if $y(n)$ takes its minimum value, the amplitude of $w(r)$ in each of these time intervals will be -1; if $y(n)$ takes its maximum value, all amplitudes will be $+1$; and for intermediate values of $y(n)$, the mean value of $w(r)$ in the corresponding sampling period will take a value proportional to $y(n)$ (Fig. 2). The UPWM signal, $w(r)$, can be generated using a digital sawtooth reference of period T (Fig. 2a) or a triangular wave of period $2T$ (Fig. 2b), both of them clocked at the rate $f_{ck} = Ff_s$. They will be called ramp UPWM (RUPWM)

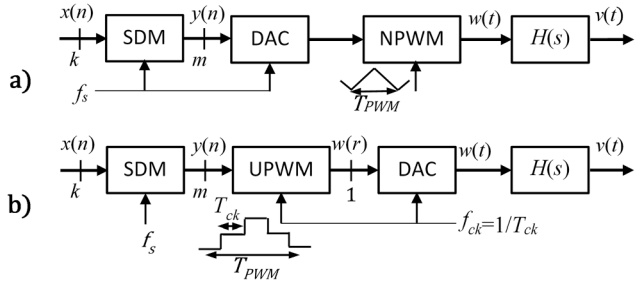

Fig. 1. Equivalent systems: a) the digital signal is converted to analog and then it is PW modulated in the CT domain and b) the signal is digitally PW modulated and then converted to the CT domain.

and $2T$-period triangular UPWM ($2T$-TUPWM), respectively. Unfortunately, the architectures of Fig. 1 achieve poor performances due to the harmonic distortion generated by the UPWM. These performances could be improved using a three-level UPWM [10] but, as previously stated, the solution proposed in this paper intends to preserve the binary nature of the output.

Under the assumption that the m-bit DAC in Fig. 1a uses T-width non-return to zero (NRZ) pulses, the NPWM input stays constant during the sampling period, and the output is given by [10]

$$v(t) = 2\sum_{k=1}^{+\infty} \frac{1}{k!}\left(\frac{T}{2}\right)^k p_k(t) \otimes h^{(k-1)}\left(t - \frac{T}{2}\right) \tag{1}$$

where $h^{(k)}(t)$ is the k^{th} time derivative of $h(t)$, $h(t)$ is the impulse response of the low-pass filter $H(s)$ in Fig. 1, and

$$p_k(t) = \sum_n y_k(n)\delta(t - \mathrm{nT}) \tag{2}$$

is the sampled signal of $y_k(t)$, where

$$y_k(n) = 1 - [-y(n)]^k \quad \text{for RUPWM} \tag{3}$$

and

$$y_k(n) = \begin{cases} [y(n)]^k & \text{n is even} \\ -[-y(n)]^k & \text{n is odd} \end{cases} \quad \text{for 2T - TUPWM} \tag{4}$$

In (4), the even periods are those in which the triangular wave has positive slope and, reciprocally, the slope is negative in the odd periods.

The distortion factors can be calculated from the above expressions. Let the input signal be a sinusoidal wave of amplitude A and frequency f_p,

$$x(t) = A\sin(2\pi f_p t) \tag{5}$$

Then, the k-th harmonic distortion factor is [10]

$$\mathrm{HD}_k = 20\log_{10}\left(\frac{A_k}{A_1}\right) = 20\log_{10}\left(\frac{(k\pi f_p\ \mathrm{TA})^{k-1}}{2^{k-1}k!}\right) \tag{6}$$

where A_k is the k^{th} harmonic amplitude of $v(t)$ at the frequency $f_k = kf_p$ and $A_1 = A$. The expression (6) can be applied to the RUPWM output but, in the case of 2T-TUPWM, it can only be applied to the odd terms. Let us observe from (4) that the k-even terms can be represented as the product of $[y(n)]^k$ by a square wave of period $2T$ and ± 1 of amplitude (with the sequence $\ldots -1,+1,-1,+1,\ldots$). Then, the even-order harmonics at low frequencies move from the signal band to a region around $f_s/2$ and, so, it is not expected to have even-order distortion. Despite this fact, the even terms can seriously affect the performances. Let's note that $y(n)$ is the output of a SDM and has a large amount of quantization noise at high frequencies. Thus, the high frequency quantization noise can be folded down at low frequency and the signal-to-(noise + distortion) ratio (SNDR) can be drastically reduced.

The analysis of a TPWM when a triangular wave has a period T, the so called 1T-TUPWM, will also be analyzed in this paper. For completeness, since the 1T-TUPWM is not treated in [10], the derivation of the distortion terms is shown in the appendix of this paper. This appendix shows that:

$$y_k(n) = \begin{cases} 0 & \text{k is even} \\ y(n) & k = 1 \\ \dfrac{[1 + y(n)]^k}{2^{k-1}} & \text{otherwise} \end{cases} \quad \text{for 1T - TUPW} \tag{7}$$

At this point two main differences are remarked, in comparison with the 2T-TUPWM case. Firstly, the k-even terms are zero and the k-odd terms are divided by 2^{k-1}. Nevertheless, as will be discussed below, adding 1 to the signal $y(n)$ can generate harmonic distortion factors of

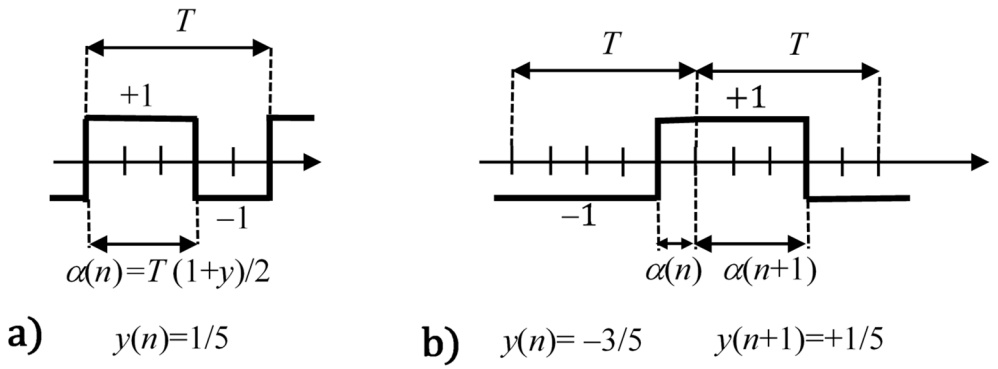

Fig. 2. UPWM output, $w(r)$, for $L = 6$ and $F = 5$: a) sawtooth and b) triangular references of period T and $2T$, respectively. The input $y \in \{-1, -3/5, -1/5, +1/5, +3/5, +1\}$

even order. Secondly, the clock frequency necessary to generate the triangular wave, $f_{ck} = 2Ff_s$, must be twice as high as in the 1T-TUPWM case; that is, the period T must be divided into a double number of time slots in order to encode $y(n)$ twice; one in the half-period when the ramp has positive slope and, the other in the remaining half-period when the slope is negative.

3. The error-correction network

3.1. The proposed architecture

In (1), term $k = 1$is the most interesting insofar as it contains the desired signal $y(n)$. The rest of terms contains powers of $y(n)$ and they contribute to errors in the D/A conversion. Among them, those that can deteriorate more the desired signal are those corresponding to $k = 2$ and 3. The expression in (1) can be written as

$$v(t) = T\left\{p_1(t) \otimes h^{(0)} + \frac{p_2(t)}{4} \otimes \left[\mathrm{Th}^{(1)}\right] + \frac{p_3(t)}{24} \otimes \left[T^2 h^{(2)}\right]\right\} + O(4) \qquad (8)$$

where, for simplicity in the notation, the k^{th} derivative of $h(t - T/2)$ has been denoted as $h^{(k)}$ and O(4) represents the sum of terms with $k \geqslant 4$.

Based on (8), in the ideal case, a correction network could be realized as depicted in Fig. 3a. The k^{th} derivative $h^{(k)}$ is implemented by replacing the low-pass filter $H(s)$ by the band-pass $s^k H(s)$, and the functions $y_k = G_k(y)$ are given by (3), (4) or (7). DACs are represented by their output pulse, the $r(t)$ function. For analytical purposes, $r(t) = \delta(t)$in (2); but in a practical realization, $r(t)$ is a NRZ pulse[1]. Based on the properties of the convolution, (8) can be expressed as

$$v(t) = w\left(t - \frac{T}{2}\right) \otimes h(t) + O(4) \qquad (9)$$

where $w(t)$ is the output of the PWM (Fig. 1)

$$w\left(t - \frac{T}{2}\right) \approx T\left\{p_1\left(t - \frac{T}{2}\right) + \frac{T\, p_2^{(1)}\left(t - \frac{T}{2}\right)}{4} + \frac{T^2 p_3^{(2)}\left(t - \frac{T}{2}\right)}{24}\right\} \qquad (10)$$

The expression (10) suggests that the derivatives can be performed in the DT domain as shown in Fig. 3b. The derivatives are implemented by the DT transfer functions $B_k(z)$. These transfer functions should be defined with the objective of minimizing the difference between both architectures in Fig. 3.

Unfortunately, there are multibit DACs in the architectures of Fig. 3 and their outputs are no longer binary signals. Furthermore, the implementation of the architectures in Fig. 3 would not be easy: multibit DACs would be required for the conversion of y_2 and y_3, which would introduce their own error terms, and good matching among the three signal paths would be crucial in order to avoid noise leakage. Moreover, the architecture in Fig. 3a requires three continuous-time filters, which would worsen the design. All of the above drastically increases the power consumption.

To solve these problems Fig. 4 shows the proposed error correction network. The error $e(n)$ in Fig. 3b can be subtracted from the signal path in the digital domain at the SDM input, as shown in Fig. 4. Since the signal gain of the SDM is equal to one, $e(n)$ is transferred to the input of the UPWM. As the signal level of $e(n)$ is much lower than $x(n)$, the new error produced by the UPWM is expected to be approximately the same in Fig. 3b and Fig. 4 and, consequently, errors $e(n)$ and that produced by

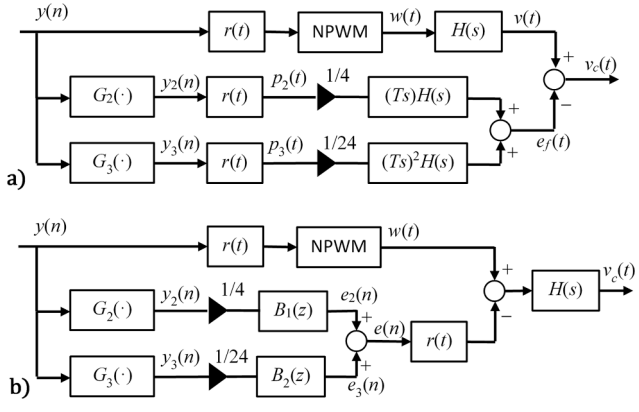

Fig. 3. Ideal correction of errors with derivatives: a) in the CT and b) DT domains, respectively.

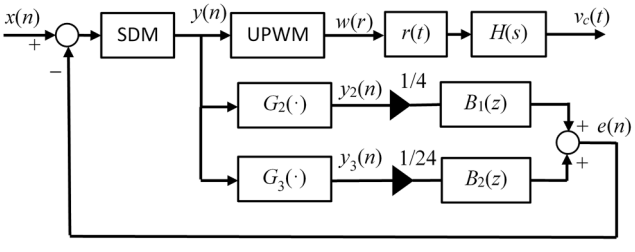

Fig. 4. Proposed error correction of the UPWM signal.

[1] That is, $r(t)$=1 for $0<t<T$ and 0 otherwise.

the UPWM in Fig. 4 will cancel each other out. The performances of the proposed error correction network will be validated by simulation in next sections.

Note that the only signal that is converted from digital to analog is $w(r)$, which is binary in nature. Therefore, the analog signal before the filter is also binary, so that it can be used to drive a class D amplifier or other devices that require a binary signal.

3.2. The transfer functions $B_k(z)$

Let note in Fig. 3b that the input of the filter $H(s)$ is the subtraction of $w(t)$ (the desired signal and error terms given in (10)) and the correction terms $e_k(t)$. The k^{th} component of the difference between the error and the correction terms is

$$\delta_k = Y_k(z)\frac{e^{-sT/2}}{2^{k-1}k!}\left[(sT)^{k-1} - \frac{e^{+sT/2}-e^{-sT/2}}{sT}B_{k-1}(z)\right] \tag{11}$$

To get to (11), let us note that the conversion of any signal $y_k(n)$through a NRZ DAC is carried out by means of the expression $Y_k(z)R(s)/T$, where $R(s) = (1-e^{-sT})/s$ is the Laplace transform of the NRZ pulse $r(t)$. The expression (11) can be reformulated as

$$\delta_k \approx Y_k(z)\frac{e^{-sT/2}}{2^{k-1}k!}(sT)^{k-1}\left[1 - \frac{B_{k-1}(z)}{(sT)^{k-1}}\right] \tag{12}$$

where the approach $(e^{+sT/2}-e^{-sT/2})/(sT) \approx 1$ has been carried out[2]. This k^{th} term approaches 0 as long as $B_k(z) \approx (sT)^k$. Nevertheless, the functions $B_k(z)$ are in the path of a closed loop (Fig. 4), so they must have at least one unit delay (z^{-1}) to avoid a non-delayed loop. In addition, for stability reasons, they must be of the finite-impulse response (FIR) type. Therefore, the terms within the parentheses in (12) cannot be cancelled; alternatively, they will be forced to approach zero in the signal band, at low frequencies. Two options are proposed, which will be so called first-order noise shaping (1st-o NS) and second-order one noise shaping (2nd-o NS), respectively.

$$\begin{aligned} &1^{st}-o \text{ NS:} && 1-\frac{B_k(z)}{(sT)^k} = 1-z^{-1} \\ &2^{nd}-o \text{ NS:} && 1-\frac{B_k(z)}{(sT)^k} = 1-2z^{-1}+z^{-2} \end{aligned} \tag{13}$$

The CT derivatives are approximated by functions of z:

$$(sT)^k \approx \begin{cases} (1-z^{-1})^k & \text{backward} \\ (1-z^{-2})^k/2^k & \text{centered} \end{cases} \tag{14}$$

Approximation in (14) also performs well at low frequencies. Other approximations of sT have been discarded in this paper. For instance, with the approximation $sT \approx 2(1-z^{-1})/(1+z^{-1})$, a pole is introduced in $B_k(z)$ which destabilizes the architecture in Fig. 4, as shown by simulations. Finally, from (13), the transfer functions can be represented as

$$B_k(z) = z^{-d}\left\{\begin{matrix} z^{-1} \\ (2z^{-1}-z^{-2}) \end{matrix}\right\}(sT)^k \tag{15}$$

where the derivative (sT) can be replaced by one of both options given in (14). For convenience, an additional delay z^{-d} has been added in (15), whose value will be selected in the next section.

4. Error correction in the triangular carrier UPWM

In that follows the well-known Error-Feedback structure [26] has been chosen as the architecture to implement the SDM. This modulator is shown in Fig. 5. To achieve second-order noise-shaping, the loop filter $F(z)$ is selected to be

$$F(z) = 2z^{-1} - z^{-2} \tag{16}$$

The modulator output is given by $Y(z) = X(z) + NTF(z)Q(z)$, where $Q(z)$ is the z-transform of the quantization noise, $q(n)$, and the noise-to-transfer function (NTF) is $NTF(z) = 1 - F(z)$. The quantizer is assumed to be of the mid-rise type (the number of levels, L, is even) with maximum and minimum values of ± 1. The signal-to-quantization noise ratio (SNQR) for an input amplitude A is given by [26]

$$\text{SNQR} = \frac{3}{2\pi^{2m}}(2m+1)\text{OSR}^{2m+1}(L-1)A^2 \tag{17}$$

where the oversampling ratio (OSR) is $f_s/(2B)$, the order of the SDM is $m = 2$, and B is the signal bandwidth.

4.1. 2T-UPWm

The system in Fig. 1 has been simulated with and without the correction networks of Fig. 4. The software used for the simulations has been Matlab® and Simulink®. The selected parameters are $B = 100$ kHz, $f_p = 9.77$ kHz, $OSR = 64$ and $A = 0.707$ (−3 dB full-scale). A second-order ($m = 2$) SDM has been chosen, and the number of bits L of the inner quantizer has been swept from 2 to 32 (even values only). There are many options in (12) for the choice of $B_k(z)$: value of d, backward or centered approximation for the CT derivatives (14), and 1st-order or 2nd-order NS cancellation (13). Among these options, two of the 1st-order NS type, and two of the 2nd-order NS type have been chosen (Table 1), which have shown to provide good results.

The SNDR obtained by simulation for different configurations is depicted in Fig. 6. The legend of this figure corresponds to: 1) Theoretical SNQR calculated from (17); 2)-5) simulated results using the correction network in Fig. 4 and the $B_k(z)$ functions given in Table 1 (from A to D); and 6) simulated results of the system of Fig. 1 without correction network.

Note that all curves converge on the value $L = 2$ (the SDM quantizer is single-bit and there is no PWM). As long as L is greater than 2, the UPWM errors produce a drastic drop in SNDR when there is no correction (curve 6). Correction networks are able of largely correcting the errors produced by the UPWM. As a matter of fact, in the worst case, curve 5, an improvement larger than 20 dB is achieved in the SNDR with respect to curve 6. In the case of 2nd-order NS, the errors practically disappear (curves 1, 2 and 3 match pretty well). We would like to remark that no harmonics were observed in the spectra of the previous simulations for the input frequency $f_p = 9.77$ kHz.

For the parameters given above, the 3rd-order distortion factor can be evaluated from (6) for $k = 3$ and its value is − 119.33 dB. This value is so low that it suggests that the correction of the third-order terms in Fig. 4 are not necessary. New simulations have been re-launched with $B_2(z) = 0$ in Fig. 4. The resulting graphs do not show significant differences with those shown in Fig. 6. Therefore, in this case the distortion network could be simplified.

To assess the ability of the proposed correction networks to suppress the harmonic distortion, a new simulation has been launched. As shown in (6), HD_3 increases with the square of the input frequency f_p. This

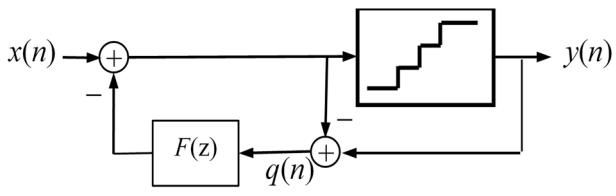

Fig. 5. Error-feedback structure.

[2] In a Taylor expansion, $(e^{+sT/2} - e^{-sT/2})/(sT) = 1 + O(h^3)$, where $h = sT$ and $O(h^3)$ are the terms of order three or greater. At low frequencies h approaches 0 and, therefore, h^2 will be much smaller than h. Simulations show that such an approximation does not produce a significant error.

Table 1
Selected $B_k(z)$ functions.

	$B_1(z)$	$B_2(z)$
A	$(2z^{-1} - z^{-2})(1 - z^{-2})/2$	$z^{-1}(2z^{-1} - z^{-2})(1 - z^{-1})^2$
B	$(2z^{-1} - z^{-2})(1 - z^{-2})/2$	$(2z^{-1} - z^{-2})(1 - z^{-2})^2/4$
C	$z^{-1}(1 - z^{-2})/2$	$z^{-2}(1 - z^{-1})^2$
D	$z^{-1}(1 - z^{-2})/2$	$z^{-1}(1 - z^{-2})^2/4$

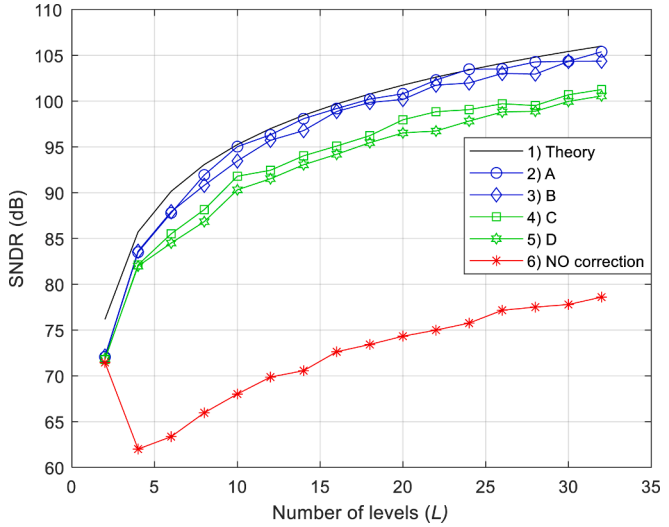

Fig. 6. Simulation results: SNDR versus L. Legend labels correspond to: 1) theoretical SNQR from (17); 2)-5) using the correction network of Fig. 4 and the $B_k(z)$ functions given in Table 1 (from A to D); and 6) Fig. 1 (without correction network).

frequency has been chosen so that its third harmonic is in the edge of the signal band; in this way the spurious free dynamic ratio (SFDR) and the SNDR drastically deteriorate. The number of quantization levels has also been chosen high ($L = 32$) to reduce the background noise. With both choices, the third harmonic is expected to be well above the noise background. Fig. 7 shows the Power Spectral Density (PSD) of the outputs, in two cases: with $B_2(z)$ given in the line A of Table 1, and with $B_2(z) = 0$(that is, without third-order correction). The theoretical HD_3 calculated from (6) is now 98 dB, value that agrees very well with the simulation result (upper graph in Fig. 7: 103–3 = 100 dB; note that additional 3 dB are subtracted due the attenuation of the Butterworth filter at its cutoff frequency $3f_p$. The 3rd-order harmonic is reduced in 11 dB when the third-order correction term is introduced (lower graph in Fig. 7). Simulated SNDRs are 98.46 and 104.34 dB for the upper and lower graphs, respectively, while the theoretical SNQR is 106 dB. The best case SFDR is as high as 111 dB. Let note that the SNDR is limited by the SFDR in the event that no 3rd-order correction is performed; in this case the SNDR (98.4 dB) is close to the SFDR (100 dB).

4.2. 1-UPWm

As stated above, the main feature of the 1T-UPWM (7), as compared to the 2T-UPWM (4), is that the even k-terms are zero and the odd k-terms are 2^{k-1} times smaller. Despite the fact that the 2nd-term error produced by the 2T-UPWM is modulated by a square wave of frequency $f_s/2$ and the signal harmonics drop out at the region of high frequency, the 2nd-order term causes the major source of error and, consequently, it is strictly necessary to use a correction network. Fortunately, in the case of 1T-UPWN, there is no 2nd-order term and the dominant source of error, the third-order term, is 4 times smaller than in the 2T-UPWM. Therefore, the 1T-UPWM performances are expected to be much better in the absence of correction.

To calculate the harmonic terms produced by the 1T-UPWM, the SDM quantization noise is discarded; that is, $y(n) = x(nT)$. Then, from (2), (7) and (10), the PWM output is proportional to

$$w(t) \propto x(t) + \frac{T^2}{24}\frac{d^2}{dt^2}\left(\frac{(1+x(t))^3}{4}\right) \tag{18}$$

where $x(t)$ is again considered to be sinusoidal of amplitude A and frequency f_p. The expression (18) can now be developed to calculate the amplitudes $A_2$and A_3 of the spectral components of frequencies $2f_p$and $3f_p$, respectively. The second- and third-order harmonic factors are:

$$HD_k = 20\log_{10}\left(\frac{A_k}{A_1}\right) = \begin{cases} 20\log_{10}\left(\dfrac{(\pi f_p\ T)^2 A}{16}\right) & k = 2 \\ 20\log_{10}\left(\dfrac{3(\pi f_p\ T)^2 A^3}{32}\right) & k = 3 \end{cases} \tag{19}$$

For the same parameters used in Fig. 6 (that is, $B = 100$ kHz, $f_p = 9.77$ kHz, $OSR = 64$ and $A = 0.707$), the harmonic factors can be calculated from (19): $HD_2 = -119.9$dB and $HD_3 = -131.4$ dB. These values are so small that the SNDR does not degrade even when there is no correction. To appreciate the effect of the harmonic distortion on architecture performances, the signal frequency is selected such that the second harmonic is in the edge of the signal band; that is, $f_p = 48.8$ kHz. The new values calculated from (19) are $HD_2 = -91.9$ dB and $HD_3 = -103.4$dB. The new *SNDR* vs. L curve is depicted in Fig. 8. The selected transfer functions are:

$$B_k(z) = \begin{cases} 0 & k = 1 \\ z^{-1}(1 - z^{-1})^2 & k = 2 \end{cases} \tag{20}$$

Note in Fig. 8 that the architecture without correction saturates whenever the SNDR approaches $-HD_2$. Unlike the 2T-UPWM case, Fig. 8. shows that the SNDR is limited by harmonic distortion rather than from the quantization noise folded down from high frequencies to the signal band by effect of the second-term error given in (4).

The spectra of the output signals obtained with the architectures of Fig. 1 (that is, without correction) and Fig. 4 are depicted in Fig. 9. To bring the harmonic terms well above the noise floor, the number of quantization levels has been chosen high enough ($L = 32$). Two comments can be highlighted. Firstly, the correction succeeds to reduce the 2nd-harmonic by about 20 dB. Secondly, the SFDR in the uncorrected architecture is 94.6 dB. This value is 3 dB greater than the theoretical value, 91.9 dB calculated from (18). This discrepancy is explained by the 3 dB attenuation of the Butterworth filter, $H(s)$, at the cutoff frequency, $B = 100$ kHz. The second harmonic frequency, 97.6 kHz, is very close to the cutoff frequency.

4.3. Limitations of the derivative approximation

The correction network relies on the approximation of the CT derivatives using difference equations (14). The approximation holds as long as the signal frequency is small enough, which is the case for an OSR of the SDM high enough. For a given OSR, the worst case occurs when the 3rd-order harmonic falls on the edge of the signal band. To assess how small the OSR can be, some simulations have been carried out. The 2T-PWM case has been chosen for its greater sensitivity to errors. The value of L has been fixed to 16 ($f_{ck} = 15f_s$) and the OSR has been swept from 4 to 30. The signal bandwidth is $B = f_s/(2OSR)$ and the

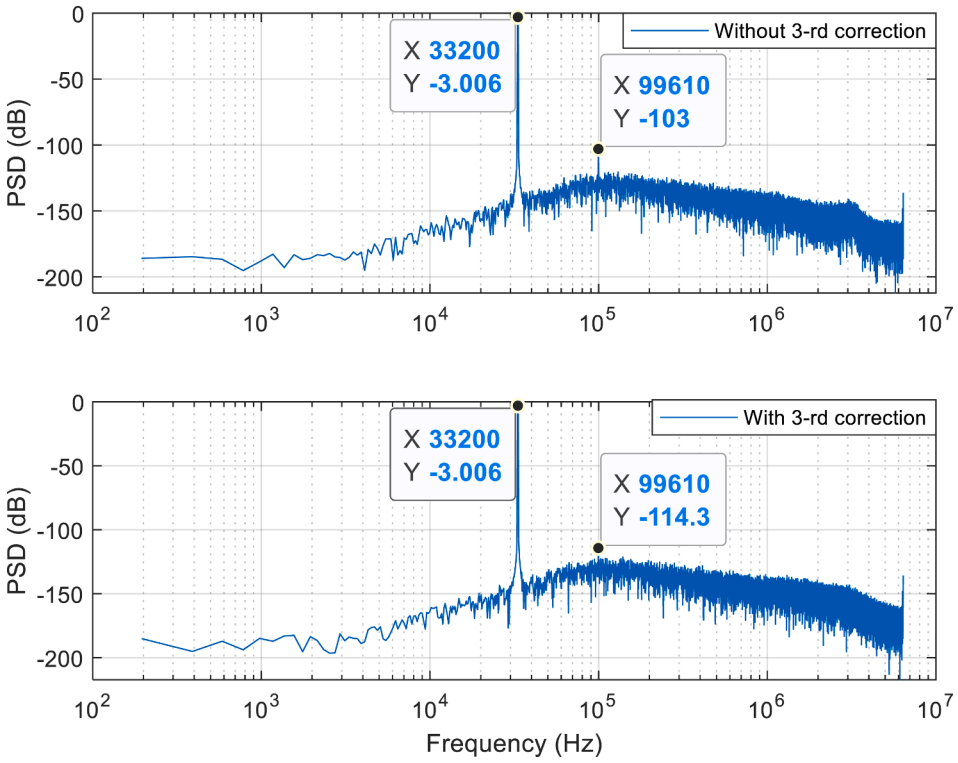

Fig. 7. PSDs obtained from Fig. 4: without (upper graph) and with (lower graph) third-order correction.

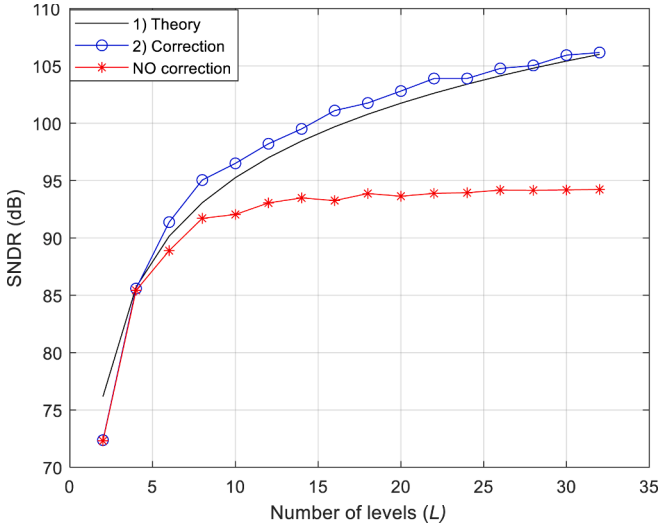

Fig. 8. Simulation results: SNDR versus L. Legend labels correspond to: 1) Theoretical SNQR from (17); 2) Fig. 4 and the functions $B_k(z)$ given in (20); and 3) Fig. 1 (without correction).

signal frequency f_p takes a value slightly smaller than $B/3$. In this way, the third harmonic is included in the calculation of the SNDR. The results are shown in Fig. 10.

As seen in Fig. 10, when the $OSR = 4$, the correction network losses its ability to cancel errors (the SNDR-A value is even smaller than that of the architecture without correction, and it is 7.6 dB smaller than the theoretical SNQR). When the OSR increases up to 7, the SFDR and the SNQR take the same value and, consequently, the quantization noise and the 3rd-order distortion equally contribute to the SNDR-A (which is 3 dB smaller than the SFDR). As long as the OSR is greater than 7 the difference between the SNQR and the SNDR of the architecture with correction will be smaller than 3 dB; the greater the OSR, the smaller this difference. Finally, for sufficiently high values of OSR, the difference in performances of both architectures (with and without correction), is of 20 dB.

5. Comparison with other correction methods

In [7], a complete digital audio system is presented, where a class-D amplifier driven by a UPWM signal is the only analog circuit. The authors use distortion correction based on the computation of the crossing point, and present experimental results that comply with audio standards. They were obtained for a 1 kHz digital input signal with an 8-bit third-order SDM operating at an OSR of 8. Simulations reveal that the proposed correction methods can achieve the same performances as those presented in [7] for the same parameters: $f_p = 1$ kHz, $B = 22.05$ kHz, $m = 3$, $L = 256$ and $f_s = 352.8$ kHz. The compensation algorithm in [7] requires 14 multiplications, 11 additions and 1 comparison per sample. On the other hand, the proposed correction techniques require 2 multiplications, some additions and a gain of 1/96 for the case of 1T-UPWM (Fig. 11). The complexity of the 2T-UPWM correction method is comparable.

Prefiltering based on Volterra series is used as distortion compensation in [22] and [23]. The same audio system of [7] was used in [22] for the purpose of testing the compensation technique. Simulation results show that performances obtained in [22] are comparable to those achieved with the methods proposed here, provided that the operating frequencies are high enough (OSR greater than 10). Related complexity, the number of multiplications per sample in [22] is 41. A much higher complexity than in [7].

Two crossing-point estimators are proposed in [24]. They are based on the maximum a posteriori (MAP) and the minimum mean squared error (MMSE) optimization methods, respectively. Simulation results show that they can outperform other crossing-point techniques, such as interpolators based on Lagrange, splines and polynomials. These MAP and MMSE methods perform well at low sampling or carrier frequencies. Unfortunately, the complexity of the methods proposed in [24] increases

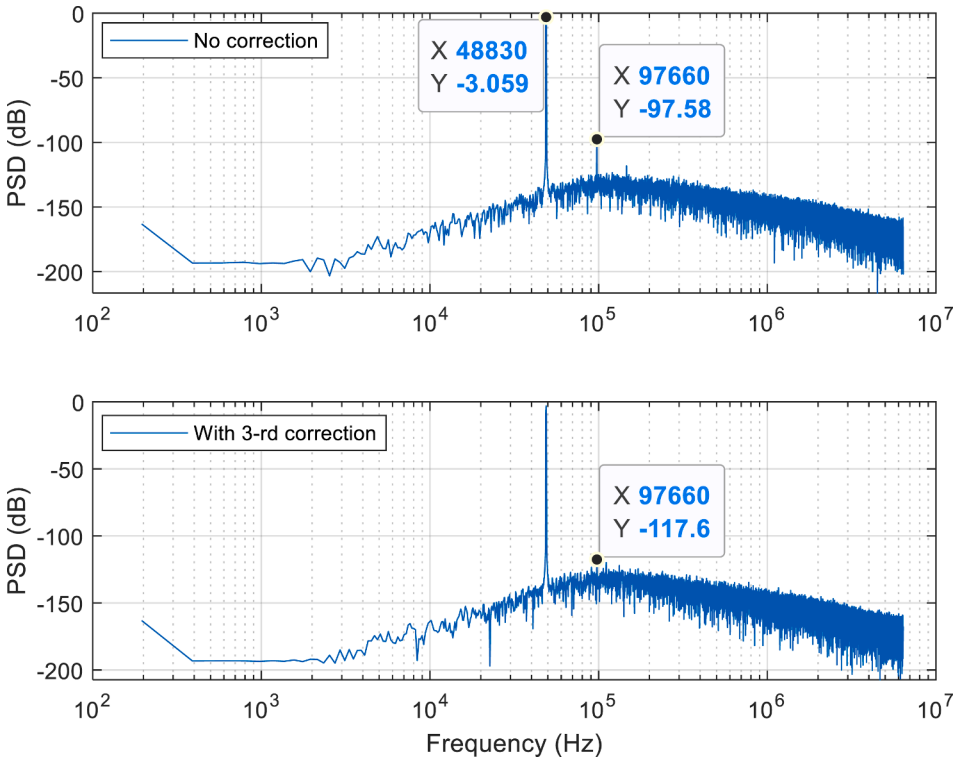

Fig. 9. PSDs obtained from Fig. 4: without (upper graph) and with (bottom graph) third-order correction.

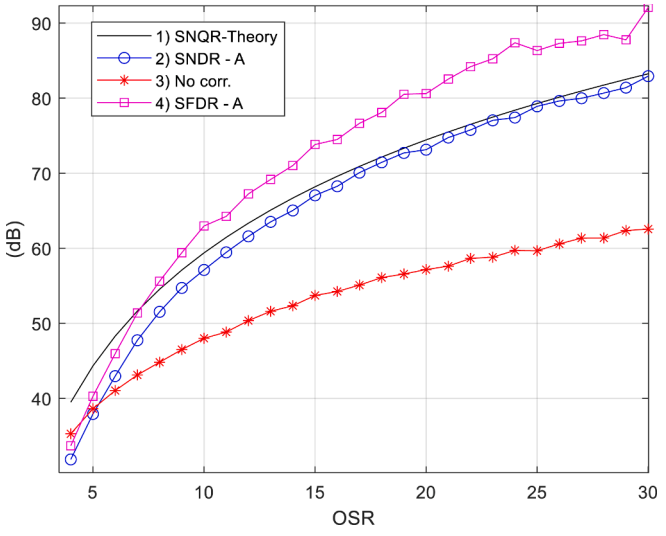

Fig. 10. SNDR and SFDR of the architecture of Fig. 4 for the case of 2T-UPWM. Legends labels correspond to: a) SNQR (17); 2) SNDR with Fig. 4 and Table 1-A; 3) SNDR with Fig. 1 and no correction; and 4) SFDR with Fig. 4 and Table 1-A.

with the square of M, unlike other previously mentioned methods whose complexity is proportional to M, where M is the number of samples taken in the interpolation. These methods are much more complex than those proposed in this paper.

In [9] three methods are proposed based on the computation of the crossing point, the so called 1st-order, 3rd-order and 5th-order PNPWM, where PNPWM stands for Pseudo-Natural PWM. The digital audio system implemented in [7] is once again used as a reference. Despite the comparable complexity of the 1T-UPWM, it outperforms the 1st-order PNPWM. The 3rd-order and 5th-order PNPWM methods achieve better performances that the methods proposed here at input signal frequencies above 4 kHz, at the cost of high computational complexity (16 additions, 5 multiplications and 1 division are required in the best case). Furthermore, in the above mentioned methods the correction network precedes the SDM where the signal word length is a large number (16 bits in the aforementioned audio system). On the contrary, in the correction methods proposed here, it succeeds the SDM (Fig. 4) where the signals are encoded with a low number of bits (8 in the aforementioned audio system, and even a lower number in most of the results presented in this paper). Taking into account that the complexity of a multiplier increases with the square value of the bit number, the methods proposed here not only introduce a lower number of multipliers, but their complexity is also much lower than in the PNPWM. Unfortunately, the proposed methods perform worse when the product $f_p \times T$ (input frequency $\times$ sampling period) increases and, consequently, a higher OSR will be required.

6. Conclusions

In this paper the errors produced by the UPWM are analyzed. From

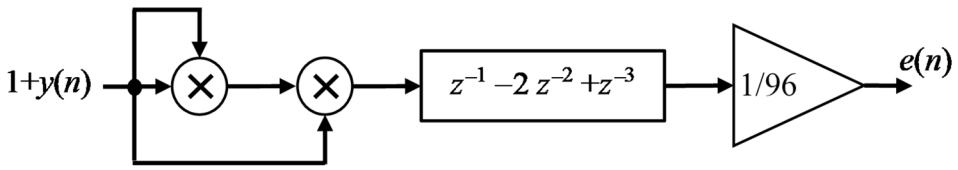

Fig. 11. Correction network for the 1T-UPWM technique.

the mathematical expression of the errors a correction network is proposed. It is implemented in the digital domain in such a way that the interface with the analog domain is a single-bit DAC, which is a simple and inherently linear circuit. Moreover, the analog output remains binary unlike what happens in other solutions proposed in the literature. This fact is an interesting property for many applications.

Two approaches, the 2T-UPWM and the 1T-UPWM, are extensively analyzed. In both cases, the cube of $y(n)$ has to be calculated, which requires two digital multipliers. Although the complexity of a digital multiplier grows with the square of the bit number, since $y(n)$ is the low-resolution output of a SDM, it is expected that the implementation of these multipliers will not be a significant overhead in the complexity of the system. The 1T-UPWM only requires the correction of the 3rd-order term while as the 2T-UPWM also requires correction of the 2nd-order term. But in the former, the digital circuit that implements the UPWM has to be clocked at twice the rate of the latter; that is, $f_{ck} = 2(L-1)f_s$ and $f_{ck} = (L-1)f_s$, respectively, where L and f_s are the number of output levels and the SDM rate, respectively.

As long as the errors are cancelled, the SNDR only depends on the OSR of the SDM and the number of levels L at its output. Provided the OSR is high enough, the simulation results show that the proposed correction network allows the system to achieve the ideal SNDR value with an acceptably high SFDR.

Declaration of Competing Interest

The authors declare that they have no known competing financial interests or personal relationships that could have appeared to influence the work reported in this paper.

Acknowledgment

Authors would like to acknowledge support from Ministerio de Ciencia, Innovación y Universidades, under the project eMIDHE RTI201-099189-B-C21.

Appendix

Fig. A1 shows the 1T-TUPWM waveform, where the output pulse is located around the center point of the n-th period. This waveform can be represented as the integration of a train of Dirac's deltas.

$$w(t) = 2\sum_n [\delta(t - t_n + \alpha_n) - \delta(t - t_n - \alpha_n)] \otimes u(t) \tag{21}$$

where $u(t)$ is the unit-step function, $t_n = nT + T/2$ is the center of the period and $\alpha_n = T\ [1 + y(n)]/4$. Then, the system output is given by

$$v(t) = w(t) \otimes h(t) = 2u(t) \otimes \sum_n [h(t - t_n + \alpha_n) - h(t - t_n - \alpha_n)] \tag{22}$$

Replacing $h(t)$ by its Taylor's expansion around the point $(t - t_n)$

$$h(t - t_n \pm \alpha) = \sum_{k=0}^{+\infty} \frac{1}{k!} h^{(k)}(t - t_n)(\pm \alpha_n)^k \tag{23}$$

where $h^{(k)}(t)$ denotes the k^{th}derivative of $h(t)$. Now, the derivative can be reduced by one order due to the operation of integration,

$$u(t) \otimes h^{(k)}(t - t_n) = h^{(k-1)}(t - t_n) \tag{24}$$

and the time shifting can be represented as a convolution with a Dirac's delta

$$h^{(k-1)}(t - t_n) = h^{(k-1)}(t - T/2) \otimes \delta(t - \mathrm{nT}) \tag{25}$$

Finally, the terms can be rearranged to get to the expression

$$v(t) = 2\sum_{k=1}^{+\infty} \frac{1}{k!} \left(\frac{T}{2}\right)^k p_k(t) \otimes h^{(k-1)}(t - T/2) \tag{26}$$

where $p_k(t)$ is given in (2) and $y_k(n)$

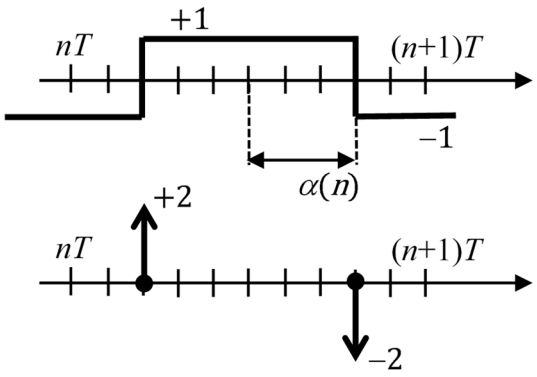

Fig. A1. 1T-TUPWM waveform in the n-th period for $y(n) = 1/5$, $L = 6$ and $F = 10$.

$$y_k(n) = \begin{cases} 0 & \text{k is even} \\ \dfrac{[1+y(n)]^k}{2^{k-1}} & \text{k is odd} \end{cases} \quad \text{for 1T - TUPWM} \tag{27}$$

The analysis started with an integration (21). Therefore, an integration constant should be added to (26). Let us observe in Fig. A1 that the UPWM signal $v(t)$ has the same mean value as $y(t)$. Therefore, a unit must be subtracted, and consequently (27) can be represented as in (7).

References

[1] Holtz J., "Pulsewidth Modulation for Electronic Power Conversion," Proceedings of the IEEE, Vol. 82, no 8, Aug. 1994. https://doi.org/10.1109/5.301684.

[2] Bowes SR, Mech MI, Mount MJ. Microprocessor control of PWM inverters. IEE Proc. Nov. 1981;128(6):293–305. https://doi.org/10.1049/ip-b.1981.0053.

[3] Martínez-heredia JM, Colodro F, Mora-Jiménez JL, Remujo A, Soriano J, Esteban S. Development of GaN Technology-Based DC/DC Converter for Hybrid UAV. IEEE Access May 2020;8:88014–25. https://doi.org/10.1109/ACCESS.2020.2992913.

[4] Vermulst BJD. Compensating Baseband Distortion of Regularly Sampled Pulsewidth Modulators for High-Precision Power Converters. IEEE Trans Power Electron July 2019;34(7):6257–63. https://doi.org/10.1109/TPEL.2018.2874362.

[5] Hiorns RE, Sandler MB. "Power digital to analog conversion using pulse width modulation and digital signal processing", IEE Proc. G, Circuits Devices Syst. 1993; 140(5):329–38. https://doi.org/10.1049/ip-g-2.1993.0055.

[6] Jun-woo Lee, Jae-shin Lee, Suki Kim, "A 2W BTL Single-Chip Class-D Power Amplifier with a Very High Efficiency for Audio Applications," in Proc. of the IEEE ISCAS, vol. V, pp. 493-496, May 2000. https://doi.org/ 10.1109/ ISCAS.2000.857479.

[7] Pascual C, Song Z, Krein PT, Sarwate DV, Midya P, Roeckner WJ. High-fidelity PWM inverter for digital audio amplification: Spectral analysis, real-time DSP implementation, and results. IEEE Trans. on Power Electronics Jan. 2003;18(1): 473–85. https://doi.org/10.1109/TPEL.2002.807102.

[8] Black HS. Modulation Theory. New York: D. Van Nostrand Co, Inc.; 1953.

[9] Goldberg Jason M. Signal Processing for High Resolution Pulse Width Modulation Based Digital-To-Analogue Conversion. PhD Thesis. University of London. Nov., 1992.

[10] Colodro F, Torralba A. Spectral analysis of Pulsewidth-Modulated Sampled Signals. IEEE Trans. on Circuits and Systems-II Aug. 2010;57(8):622–6. https://doi.org/ 10.1109/TCSII.2010.2048483.

[11] Goldberg JM, Sandler MB. Pseudo-natural pulse width modulation for high accuracy Digital-to-Analog Conversion. IEE Electronics Letters Aug. 1991;27(16): 1491–2. https://doi.org/10.1049/el:19910933.

[12] E. Roza, "Analog-to-digital conversion via duty-cycle modulation," IEEE Trans. on Circuits and Systems II, vol. 44, no. 11, pp. 907–914, Nov. 1997. https://doi.org/ 10.1109/82.644044.

[13] S. Ouzounov, H. Hegt, and A. van Roermund, "Sigma-delta modulators operating at a limit cycle," IEEE Trans. on Circuits and Systems II, vol. 53, Iss. 5, pp. 399-403, May 2006. https://doi.org/10.1109/TCSII.2006.870212.

[14] F. Colodro, A. Torralba, M. Laguna, "Continuous-Time Sigma–Delta Modulator with an Embedded Pulsewidth Modulation," IEEE Trans. on Circuits and Systems I, vol. 55, Iss. 3, pp. 777-785, Apr. 2008. https://doi.org/10.1109/ TCSI.2008.919764.

[15] L.H. Corporales, E. Prefasi, E. Pun, and S. Paton, "A 1.2-MHz 10-bit Continuous-Time Sigma–Delta ADC Using a Time Encoding Quantizer," IEEE Trans. on Circuits and Systems II, Vol. 56, Iss. 1, pp. 16-20, Jan. 2009. https://doi.org/10.1109/ TCSII.2008.2008524.

[16] Colodro F, Torralba A. New continuous-time multibit sigma-delta modulators with low sensitivity to clock jitter. IEEE Trans. on Crcuits and Systems-I Jan. 2009;56 (1):74–83. https://doi.org/10.1109/TCSI.2008.922178.

[17] Li H, Breyne L, Kerrebrouck JV, et al. A 21-GS/s single-bit second-order delta-sigma modulator for FPGAs. IEEE Trans. Circuits Syst. 2019;66:482–6. https://doi.org/10.1109/TCSII.2018.2855962. doi: 10.1109/TCSII.2018.2855962.

[18] Holmes D.G, Cheng L, Shimaponda-Nawa M, Familua A.D, and Abu-Mahfouz A.M. Modelling noise and pulse width modulation interference in indoor visible light communication channels. AEU Int. Jour. of Electron. and Commun., July, 2019; vol. 106, https://doi.org/10.1016/j.aeue.2019.04.014.

[19] Khorrami A, Afifi A, Ghezelayagh MH. Design and analysis of loran transmitter based on PWM switching and OMOE indicator. AEU Int. Jour. of Electron. and Commun. November 2019;111. https://doi.org/10.1016/j.aeue.2019.152879.

[20] Colodro F, Martinez-Heredia JM, Mora JL, Torralba A. Open loop sigma-delta modulators for digital-to-analog converters with high speed improving using time interleaving. AEU Int. Jour. of Electron. and Commun. October 2020;125. https://doi.org/10.1016/j.aeue.2020.153394.

[21] Seebacher D, Singerl P, Schuberth C, Dielacher F, Reynaert P, Wolfgang Bösch W. Reduction of Aliasing Effects of RF PWM Modulated Signals by Cross Point Estimation. IEEE Trans. on Circuits and Systems-I February 2013;61(2):3184–92. https://doi.org/10.1109/TCSI.2014.2334914.

[22] Aase, S. O. (2014). Digital removal of pulse-width-modulation-induced distortion in class-D audio amplifiers. IET Signal Processing, August, 2014; 8(6), 680-692. https://doi.org/10.1049/iet-spr.2013.0383.

[23] Aase, S. O. (2012). A prefilter equalizer for pulse width modulation. Signal processing, October, 2012; 92(10), 2444-2453. https://doi.org/10.1016/j. sigpro.2012.03.006.

[24] Smecher, G., & Champagne, B. (2011). Optimum crossing-point estimation of a sampled analog signal with a periodic carrier. Signal processing, August 2011; 91 (8), 1951-1962. https://doi.org/10.1016/j.sigpro.2011.02.018.

[25] Hausmair K, Chi S, Singerl P, Vogel C. Aliasing-Free Digital Pulse-Width Modulation for Burst-Mode RF Transmitters. IEEE Tans. on Circuits and Systems-I November 2014;60(2):415–27. https://doi.org/10.1109/TCSI.2012.2215776.

[26] Norsworthy SR, Schreier R, Temes GC. Delta-Sigma Data Converters: Theory, Design and Simulation. New York: IEEE Press; 1997.

Francisco Colodro received his Telecommunications Engineering degree from the Universidad de Vigo, Spain, in 1992, and his Ph.D. degree from Universidad de Sevilla, Spain, in 1997. He is currently Associate Professor in the Department of Electronic Engineering of this University. His research interests include analog-to-digital and digital-to-analog conversion, sigma–delta modulators, and microelectronic circuits and systems with application to control, aeronautics and communications.

Juana M. Martinez-Heredia received her Telecommunications Engineering and Ph.D. degrees from Universidad de Sevilla, Spain, in 1999 and 2006, respectively. Since 1999, she has been with the Department of Electronic Engineering of this University, where she is an Assistant Professor. Her research interests include low-voltage low-power analog circuit design, analog and mixed-signal design, and design of circuits for aircrafts and UAVs

José Luis Mora-Jiménez received his M.S. and Ph.D. degrees in Industrial Engineering from Universidad de Sevilla, Spain, in 1992 and 2001, respectively. He is currently an Assistant Professor in the Department of Electronic Engineering of this University. His current research areas are digital design, modeling and control of power converters, multilevel converters, and sensor-less motor drives.

Antonio Torralba (M'89-SM'02) has a Ph.D. in Electrical Engineering from University of Sevilla (1985). He joined the Electronic Engineering Department of this University in 1983, becoming Full Professor in 1996. He is also with the Laboratory of Engineering for Energy and Environmental Sustainability of the University of Seville. He has published more than 100 papers in Journals and Transactions. His research interest is in analog and mixed design.